A nonlinear asymptotic model for the inertial flow at a fluid-porous interface

Philippe Angot, Benoît Goyeau, J Alberto Ochoa-Tapia

A nonlinear asymptotic model for the inertial flow at a fluid-porous interface

Philippe Angot[a,*], **Benoît Goyeau**[b], **and J. Alberto Ochoa-Tapia**[c]

[a] *Aix-Marseille Université, Institut de Mathématiques de Marseille, CNRS UMR-7373, Centrale Marseille, 39 rue F. Joliot-Curie, 13453 Marseille cedex 13, France*
[b] *Ecole Centrale-Supélec, Université Paris-Saclay, EM2C, CNRS UPR-288, 8-10 rue Joliot-Curie, 91190 Gif-sur-Yvette, France*
[c] *Universidad Autónoma Metropolitana-Iztapalapa, Departamento de Ingeniería de Procesos e Hidráulica, Mexico 09340 D.F., Mexico*

Abstract

An original nonlinear multi-dimensional model for the inertial fluid flow through a fluid-porous interface is derived by asymptotic theory for arbitrary flow directions. The interfacial region between the pure fluid and the homogeneous porous region is viewed as a thin transition porous layer characterized by smoothly evolving heterogeneities. The asymptotic analysis applied to the homogenized Navier-Stokes equations in this thin heterogeneous porous layer leads to nonlinear momentum jump conditions at the equivalent dividing interface. These jump conditions involve slip and friction coefficients whose dependence on porosity are analyzed. Moreover, we show that the resulting Navier-Stokes/Darcy-Forchheimer macroscale coupled model is globally dissipative in the porosity range $0 < \phi_p \leq 0.95$, which also contributes to its physical relevance. To our knowledge, this innovative asymptotic model is the first nonlinear multi-dimensional model proposed in the literature for the inertial flow with arbitrary flow directions at a permeable interface. Besides, it clearly opens new perspectives to study turbulent flows at the fluid-porous interface.

Keywords: Fluid-porous inertial flow, Asymptotic analysis, Nonlinear jump interface conditions, Slip and friction coefficients, Navier-Stokes/Darcy-Forchheimer model, Globally dissipative model

1. Main objectives and highlights

The momentum transport at the interface between a fluid and a permeable region is present in a large variety of industrial applications (dendritic solidification of multi-component mixtures, fuel cell, oil recovery, separation processes, etc), but also in environmental situations or for water resources (surface or subsurface hydrology, interaction atmosphere/canopy, benthic boundary layers, etc) or biological systems (bone growth, biofilms, cell proliferation, etc). We refer to the recent paper [1] and the references therein for many examples of application. Due to the different characteristic length scales involved in these heterogeneous configurations, the momentum transport analysis is often performed at the macroscopic scale where the concept of interface is actually related to the nature of the average representation. From the pioneering work of Beavers and Joseph [2], two macroscopic modeling approaches have been used. The single-domain approach considers the interfacial region as a thin transition porous layer (see Fig. 1) where the averaged properties (porosity, permeability) are continuously spatially dependent (evolving heterogeneities). On the other hand, the two-domain approach considers a fictive interface (see Fig. 2) where explicit jump boundary conditions must be expressed. It is worth mentioning that these jump conditions result from an integration of the momentum transport on the thin transition layer of the single-domain approach [3, 4].

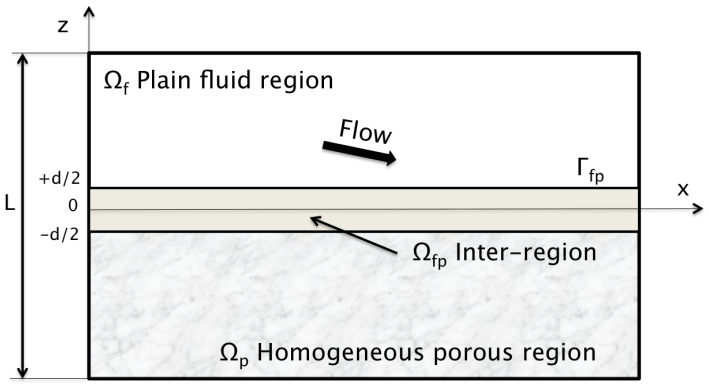

Figure 1: One-domain modeling: continuous inter-region.

Different studies have been devoted to the derivation of these jump conditions for non-inertial one-dimensional

*Corresponding author
Email address: philippe.angot@univ-amu.fr (**Philippe Angot**)

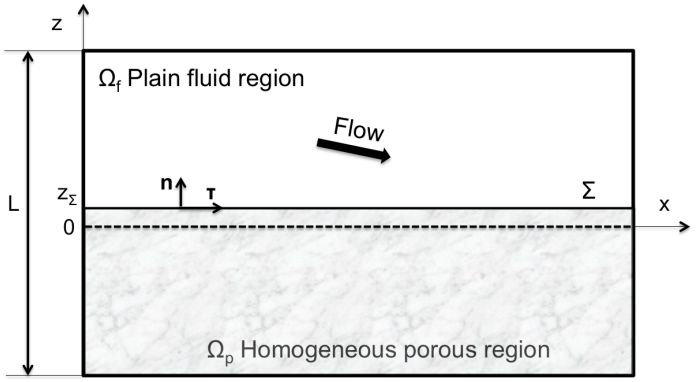

Figure 2: Two-domain modeling: interface Σ located at $\xi := z_\Sigma/d$.

channel flows parallel to the porous layer [2–10]. Using an asymptotic modeling as for thin fractures in porous media [11], the present authors have recently derived in [12] jump conditions for a general two- or three-dimensional non-inertial viscous flow and arbitrary flow directions at a permeable interface.

However, many applications concern flow regimes where inertial effects have to be considered [13]. A few papers address the inertial flows at a fluid-porous interface by numerical simulations at the macroscopic scale [14, 15] or at the pore scale [16–22], but mainly restricted to the 1-D channel case. To the best of our knowledge, there exists no general interface model for the multi-dimensional inertial flow and arbitrary flow directions [13]. Hence, the macroscopic description of the inertial flow through a permeable interface is still a challenging open problem in fluid dynamics.
This is the objective of the present theoretical study where the asymptotic analysis [12], applied here to the homogenized Navier-Stokes equations in the thin transition porous layer, yields an original nonlinear multi-dimensional model for the inertial flow over a permeable medium. Moreover, we show that the total work of the inertial forces in the fluid and porous domains has always a positive contribution at the interface to the dissipation of kinetic energy inside the whole system.

The paper is organized as follows. Section 2 details the model equations governing the flow in the fluid and permeable regions. In Section 3, we derive the asymptotic model for the inertial flow: only the contribution of all the additional nonlinear and inertial terms is detailed, including the cases of both weak or strong inertia. The resulting nonlinear interface conditions are discussed in Section 4. Finally, the mechanical energy balance is derived in Section 5 which suggests some concluding remarks. The present analysis is carried out in detail for the porosity range $0 < \phi_p \leq 0.95$, but Remark 5 gives some hints on how to generalize it for larger porosities $\phi_p > 0.95$.

2. Fluid-porous inertial flow models

Let us consider a two-dimensional[1] bounded domain $\Omega \subset \mathrm{R}^2$ composed of a pure fluid region Ω_f of constant mass density ρ, dynamic viscosity μ and a saturated porous medium $\Omega_{fp} \cup \Omega_p$ separated by a physical interface Γ_{fp}; see Figure 1. The homogeneous part of the porous region Ω_p is characterized by its constant porosity ϕ_p (volume fraction of fluid) and permeability tensor $\boldsymbol{K}_p$ with $K_p := \|\boldsymbol{K}_p\|$, whereas $\phi_p \leq \phi := \phi(x,z) \leq 1$ and $\boldsymbol{K} := \boldsymbol{K}(\phi)$ are respectively the spatially dependent porosity and permeability tensor of the non-homogeneous interfacial transition layer Ω_{fp}. The porosity ϕ inside Ω_{fp} is assumed to vary smoothly from ϕ_p to 1 (for the pure fluid) over the thickness $d \ll L$, where L represents the characteristic length scale of the system (at least $L \sim 100d$ [3] or far more). For example, Kozeny-Carman's formula [23] for $K_p(\phi_p)$ correlation confirmed in [24] is classically used for granular media, whereas Happel-Langmuir's one [25] or others gathered in [26] are more suitable for fibrous materials.

The asymptotic analysis is based on the integration of the momentum transport over the thickness d of Ω_{fp} giving rise to jump conditions at a fictive interface Σ whose location inside Ω_{fp} is not known *a priori*; here located at the dimensionless height $-1/2 \leq \xi := z_\Sigma/d \leq 1/2$ in Fig. 2. The thin transition layer Ω_{fp} is then replaced by the interface[2] Σ associated with suitable jump interface conditions.

2.1. Flow models with inertia

The flow models without inertia are discussed in detail in [12] for the Stokes/Brinkman or Stokes/Darcy problems. The present analysis concerns the flow models with inertia. Here, we consider the so-called Navier-Stokes/Darcy-Forchheimer fluid-porous problem in the range of porosity $0 < \phi_p \leq 0.95$. Under these conditions, the steady form of the inertial incompressible viscous flow in the fluid-porous system Ω is governed at the macroscopic scale by the fol-

[1] For the sake of clarity, the present asymptotic model is derived hereafter for the 2-D flow, although the extension to 3-D is quite straigthforward since all the tangential derivative and possibly curvature terms are neglected up to first-order in $O(d/L)$.

[2] The reader should be careful that the notations of Ω_f and Ω_p are not obviously consistent between Fig. 1 and Fig. 2, but this is for the practical sake of simplicity and convenience.

lowing set of equations:

$$\boldsymbol{\nabla}\cdot\boldsymbol{v} = 0 \quad \text{in } \Omega \quad (1)$$

$$\boldsymbol{\nabla}\cdot(\rho\,\boldsymbol{v}\otimes\boldsymbol{v}) - \mu\,\Delta\boldsymbol{v} + \nabla p = \rho\,\boldsymbol{f} \quad \text{in } \Omega_f \quad (2)$$

$$\frac{1}{\phi}\,\boldsymbol{\nabla}\cdot\left(\frac{\rho}{\phi}\,\boldsymbol{v}\otimes\boldsymbol{v}\right) - \boldsymbol{\nabla}\cdot\boldsymbol{\sigma}(\boldsymbol{v},p) + \mu\,\boldsymbol{K}^{-1}\cdot\boldsymbol{v} + \frac{\rho}{\sqrt{K_p}}\,|\boldsymbol{v}|\,\boldsymbol{\kappa}(\phi)\cdot\boldsymbol{v} = \rho\,\boldsymbol{f} \quad \text{in } \Omega_{fp} \quad (3)$$

$$\mu\,\boldsymbol{K}_p^{-1}\cdot\boldsymbol{v} + \frac{\rho}{\sqrt{K_p}}\,|\boldsymbol{v}|\,\boldsymbol{\kappa}(\phi_p)\cdot\boldsymbol{v} + \nabla p = \rho\,\boldsymbol{f} \quad \text{in } \Omega_p \quad (4)$$

where the symbol $\otimes$ represents the tensor product. In the above system, $\boldsymbol{f}$ is a force per mass unit, $\boldsymbol{\kappa}$ is the Dupuit-Forchheimer tensor and $\boldsymbol{\sigma}(\boldsymbol{v},p)$ represents the stress tensor for a Newtonian fluid, $\boldsymbol{v}$ being the velocity and p the pressure, defined by:

$$\begin{aligned}\boldsymbol{\sigma}(\boldsymbol{v},p) &:= \widetilde{\mu}\left(\nabla\boldsymbol{v} + \nabla\boldsymbol{v}^T\right) - p\,\boldsymbol{I}\\ &= \frac{\mu}{\phi}\left(\nabla\boldsymbol{v} + \nabla\boldsymbol{v}^T\right) - p\,\boldsymbol{I},\\ &\quad \text{with} \quad \phi = 1 \ \text{ in } \ \Omega_f, \quad \phi = \phi_p \ \text{ in } \ \Omega_p,\end{aligned} \quad (5)$$

where $\boldsymbol{I}$ denotes the identity tensor.

In the above system, equation (1) represents the mass conservation in the whole domain Ω where $\boldsymbol{v}$ is the superficial average velocity, also called the filtration velocity (the velocity of the solid skeleton being here null). The pressure p refers to the intrinsic average pressure (the pressure inside the solid skeleton being non-defined). Hence, the variables $\boldsymbol{v}, p$ are physically measurable quantities at the macroscopic scale. Here, it is interesting to note that the momentum transport models for the two stratified porous regions $\Omega_{fp}\cup\Omega_p$ are obtained from the so-called Navier-Stokes/Darcy-Forchheimer equation (3) which has been derived using a volume averaging method [27–29] in the context of the one-domain approach. We also refer to [30] for a more recent and precise derivation of this equation in the case of evolving heterogeneities. All the terms in equation (3) arising from the upscaling procedure have to be kept due to evolving heterogeneities but their contribution obviously depends on the porosity values ($\phi_p \le \phi \le 1$). For instance, in the pure fluid region Ω_f, $\phi \to 1$, $\|\boldsymbol{K}(\phi)\| \to +\infty$ and $\boldsymbol{\kappa}(\phi) \to 0$, therefore the two friction terms including the permeability become negligible and equation (3) asymptotically tends towards the Navier-Stokes equation (2).

In the homogeneous porous bulk Ω_p, the Darcy-Forchheimer equation (4) is obtained by considering equation (3) when $\phi \to \phi_p$, therefore valid in Ω_p and then, both the Brinkman viscous term with respect to the Darcy drag and the Navier-Stokes nonlinear term with respect to the Dupuit-Forchheimer quadratic term are discarded. As explained a little further in Sec. 2.2, these approximations are clearly valid at the macroscopic scale in the porosity range $0 < \phi_p \le 0.95$. In other words, equation (3) asymptotically tends towards equation (4) at the porous interface between Ω_{fp} and Ω_p where $\phi = \phi_p$. Under these conditions, we have natural continuity of both the velocity and stress vectors on Γ_{fp}; see [3, 31]. This also holds at the porous interface between Ω_{fp} and Ω_p, *i.e.* at the bottom of the transition layer Ω_{fp} since the Brinkman boundary layer is fully included inside Ω_{fp}; see [32, 33].

The quadratic form of Dupuit-Forchheimer's inertial friction is confirmed by many studies in the strong inertia regime, e.g. theoretical works [28, 34], direct numerical simulations in ordered [35] or random porous media [36]. The correlation of Ergun's coefficient $\kappa(\phi)$ [37] was confirmed in [38], also in good agreement with the analytical approach proposed in [39], although some others are discussed in [40–42]. These correlations are recalled in Appendix B.

2.2. Justification of the approximations

In order to justify the approximations made in Sec. 2.1, it is useful to plot the ratio between the orders of magnitude of Brinkman's viscous term and Darcy's drag term. Let us use for the homogeneous and isotropic porous medium of porosity ϕ and permeability $K(\phi)$, the well-known Kozeny-Carman's formula [23] confirmed in [24] for the absolute permeability of random packed beds of spherical particles for granular materials. This reads as below, d_p being the mean diameter of particles and η being the size of representative unit cell:

$$\begin{aligned}\text{with :} \quad 1-\phi &= \frac{\pi}{6}\left(\frac{d_p}{\eta}\right)^3,\\ K(\phi) &\simeq \frac{d_p^2\,\phi^3}{180\,(1-\phi)^2} \simeq 0.00855\,\frac{\eta^2\,\phi^3}{(1-\phi)^{4/3}}.\end{aligned} \quad (6)$$

Finer correlations for many other permeable media, like fibrous materials with arrays of cylinder rods aligned or normal to the flow, are gathered and discussed in [26, 43]. For example, they reported the formula below of Langmuir (1942) and confirmed by Happel (1959), d_f being now the characteristic diameter of fibers :

$$K(\phi) \simeq \frac{d_f^2}{16\,(1-\phi)}\left(-\ln(1-\phi) - \frac{3}{2} + 2\,(1-\phi)\right) \quad (7)$$

Figure 3 shows the well-known variation of the dimensionless permeability with the porosity for both granular and fibrous materials.

Then with $\widetilde{\mu} = \mu/\phi$ in Eq. (3) with (5), it is useful to compare the ratio $\mathrm{R}_{B/D}$ of the orders of magnitude between Brinkman's viscous term $\boldsymbol{\nabla}\cdot\widetilde{\mu}\,(\nabla\boldsymbol{v} + \nabla\boldsymbol{v}^T)$ of order $O(\widetilde{\mu}\,V/L^2)$ and Darcy's drag term $\mu\,\boldsymbol{K}^{-1}\cdot\boldsymbol{v}$ of order $O(\mu\,V/K(\phi))$ using Kozeny-Carman's correlation (6). Thus, we get :

$$\mathrm{R}_{B/D} = \frac{d_p^2}{L^2}\,\frac{\phi^2}{180\,(1-\phi)^2}. \quad (8)$$

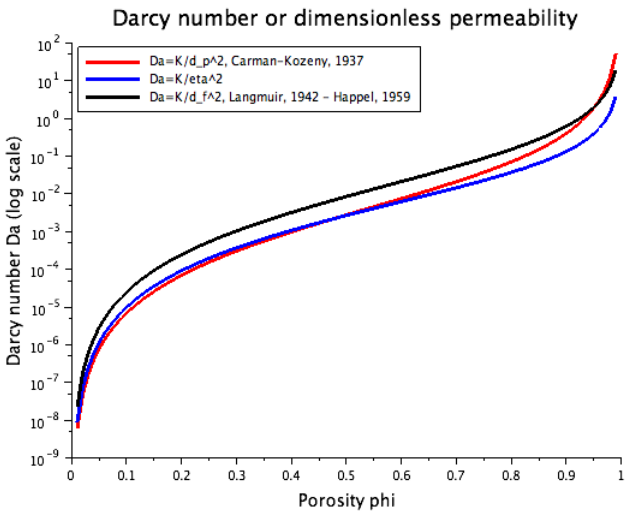

Figure 3: Darcy number (dimensionless permeability) $\mathrm{Da} = K(\phi)/d_p^2$ (red) or $\mathrm{Da} = K(\phi)/\eta^2$ (blue) with Kozeny-Carman's formula Eq. (6) and $\mathrm{Da} = K(\phi)/d_f^2$ (black) with Langmuir-Happel's formula Eq. (7).

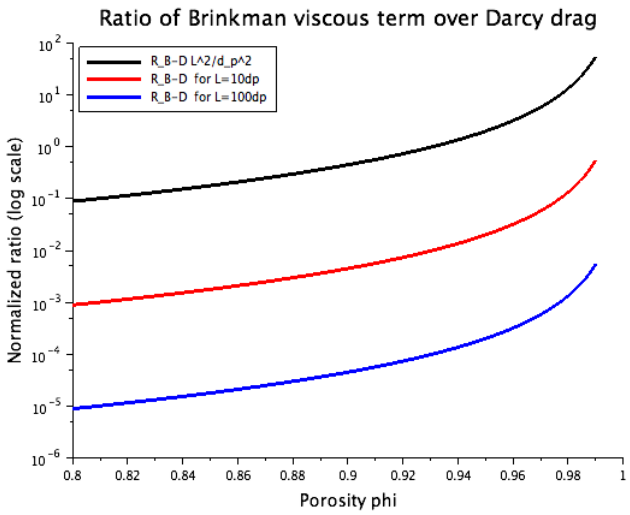

Figure 4: Ratio $\mathrm{R}_{B/D}$ of Brinkman's viscous term over Darcy's drag Eq. (8) in the porosity range $0.80 \leq \phi < 1$: $L = d_p$ (black), $L = 10\,d_p$ (red) and $L = 100\,d_p$ (blue).

Here, V denotes a characteristic scale of velocity and Kozeny-Carman's formula (6) is used for the correlation $K(\phi)$. The graph of $\mathrm{R}_{B/D}$ is plotted in Fig. 4 for different macroscopic scales L/d_p in the range of porosity $0.80 \leq \phi < 1$. Hence, at a macroscopic scale of the whole fluid-porous system usually such that $L = O(100\,d_p)$ at least or far more, the Brinkman viscous term can be clearly neglected for $\phi \leq 0.95$, except for highly permeable media as fibrous ones when we usually have $\phi > 0.98$. In particular, this term must be kept in the interfacial porous layer Ω_{fp} of thickness $d = O(d_p)$ and where ϕ varies continuously from ϕ_p to 1. Indeed, when $\phi \to 1$, we have $\mathrm{R}_{B/D} \to \infty$ and the Darcy-Brinkman equation recovers the Stokes one.

Let us now detail how to generalize the momentum transport equation to include the inertial effects at the macroscopic scale. The suggestion that the one-dimensional form be modified by the addition of a term proportional to $\rho\,\boldsymbol{v}^2$ dates back to Dupuit (1863) [44], but the modified equation is usually associated to Forchheimer (1901) [45]. This is confirmed by many experimental results [37, 38, 46–50] or numerical results [35, 36, 40–42, 51–53]. Moreover, upscaling methods as homogenization [54–56] or volume averaging [28, 34, 57, 58] prove the quadratic behaviour of the macroscopic inertial effect when the Navier-Stokes equations govern the flow at the microscopic scale.
Forchheimer and others [52, 59–61] have also included a term proportional to $|\boldsymbol{v}|^2\,\boldsymbol{v}$, but this cubic transition regime from the non-inertial linear regime seems to appear only for weak inertia and shortly for the 3-D flow in random media [41, 42, 62, 63].

For an isotropic homogeneous porous medium with a constant porosity ϕ and permeability $K = K(\phi)$, the Navier-Brinkman-Dupuit-Forchheimer equation reads as follows after [28, 64–66]:

$$\frac{\rho}{\phi^2}\,(\boldsymbol{v}\cdot\nabla)\boldsymbol{v} - \widetilde{\mu}\,\Delta\boldsymbol{v} + \frac{\mu}{K}\,\boldsymbol{v} + \frac{\kappa(\phi)}{\sqrt{K(\phi)}}\,\rho\,|\boldsymbol{v}|\,\boldsymbol{v} + \nabla p = \rho\,\boldsymbol{f} \quad (9)$$

where the non-dimensional scalar function $\kappa(\phi) > 0$ in Dupuit-Forchheimer's quadratic inertial friction strongly depends on the porosity ϕ, $|\boldsymbol{v}|^2 := \boldsymbol{v}\cdot\boldsymbol{v}$ being the square of the Euclidean norm of vector $\boldsymbol{v}$. For example, [64] suggested the mean value $\kappa \simeq 0.55$, whereas [37] proposed from his experimental data a $\kappa - \phi$ correlation given in Appendix B. Later, [38] confirmed a very close correlation for $\kappa(\phi)$ as:

$$\kappa(\phi) \simeq 1.80\,\frac{(1-\phi)^{1/2}}{\phi^3}. \quad (10)$$

This is also in good agreement with the analytical approach proposed in [39]. Then, together with Kozeny-Carman's formula 6, it gives:

$$\frac{\kappa(\phi)}{\sqrt{K(\phi)}} \simeq 24.15\,\frac{(1-\phi)^{3/2}}{d_p\,\phi^{9/2}}. \quad (11)$$

Other correlations exist from various experimental data or numerical results supplied in Appendix B, e.g. [40, 41, 46], giving a large disparity or even some discrepancy as shown in Fig. 5. However, it is important to mention that all these correlations are not calibrated for the same media, ordered or random, and some result from experimental measurements and others from numerical simulations. Besides, they are not all valid in the whole range of porosity $0 < \phi < 1$. For instance, $\kappa(\phi)$ does not tend to 0 when

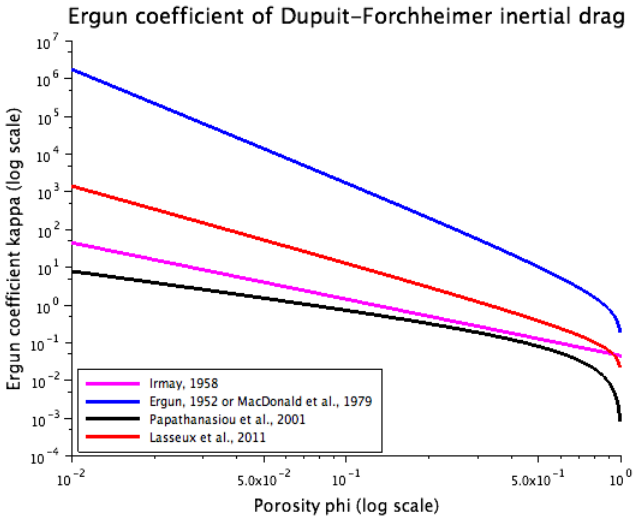

Figure 5: Ergun's coefficient $\kappa(\phi)$ of Dupuit-Forchheimer's inertial drag in Eq. (9) in the range $0 < \phi \leq 1$ with the $\kappa - \phi$ correlations summarized in Appendix B: Eq. (B.1) or (B.3) (blue), Eq. (B.5) (red), Eq. (B.2) (magenta) and Eq. (B.4) (black).

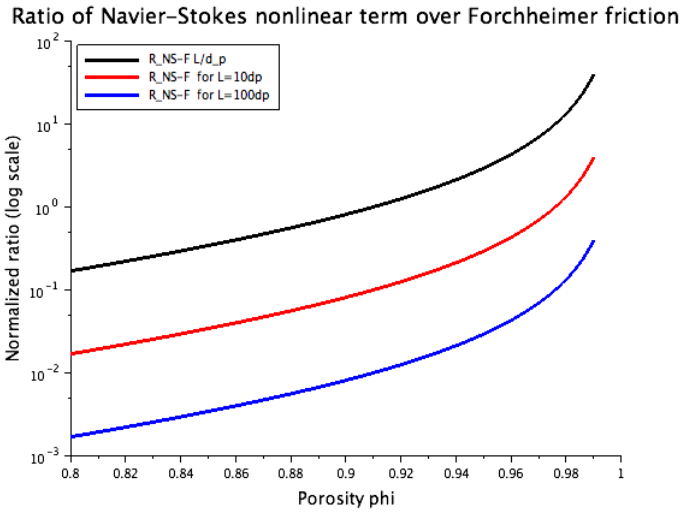

Figure 6: Ratio $\mathrm{R}_{NS/F}$ of the Navier-Stokes nonlinear term over Dupuit-Forchheimer's inertial friction Eq. (12) in the porosity range $0.80 \leq \phi < 1$: $L = d_p$ (black), $L = 10\,d_p$ (red) and $L = 100\,d_p$ (blue).

$\phi \to 1$ in [46] and the results of [41] are limited to the range $0.3 \leq \phi \leq 0.75$.

In such a way, when $d_p \to 0$ and $\phi \to 1$, we have using Kozeny-Carman's relation $K(\phi) \to +\infty$, and the inertial resistance factor $\kappa(\phi)/\sqrt{K(\phi)} \to 0$ with Eq. (11) or with other $\kappa - \phi$ correlations. Therefore, since we have also $\widetilde{\mu} \to \mu$, the Navier-Stokes equation is fully recovered with Eq. (9) which justifies the presence of the Navier-Stokes nonlinear term. Indeed, this term in Eq. (9) actually comes from the volume averaging process of the Navier-Stokes equation at the microscopic scale, as developed by Whitaker (1996) [28].

Nevertheless, for many real porous media, the Navier-Stokes nonlinear term is shown to be negligible with respect to Dupuit-Forchheimer's inertial term, and thus, it is often omitted when $\phi \leq 0.95$. Indeed, the following approximation holds with (11), except for a large porosity since $\kappa(\phi)/\sqrt{K(\phi)} \to 0$ when $\phi \to 1$:

$$\left|\frac{\rho}{\phi^2}\,(\boldsymbol{v}\cdot\nabla)\boldsymbol{v}\right| = O\left(\frac{\rho\,V^2}{\phi^2\,L}\right) \ll \frac{\rho}{\sqrt{K_d}}\,|\boldsymbol{v}|\,\boldsymbol{\kappa}(\phi)\cdot\boldsymbol{v} = O\left(\frac{\rho\,V^2\,\kappa(\phi)}{\sqrt{K(\phi)}}\right).$$

Using Eq. (11), the ratio $\mathrm{R}_{NS/F}$ of these quantities reads:

$$\mathrm{R}_{NS/F} \simeq \frac{d_p}{L}\,0.0414\,\frac{\phi^{9/2}}{(1-\phi)^{3/2}}. \qquad (12)$$

The graph of $\mathrm{R}_{NS/F}$ is plotted in Fig. 6 for different macroscopic scales L/d_p in the range of porosity $0.80 \leq \phi < 1$. This shows that the Navier-Stokes nonlinear term cannot be neglected when $\phi \to 1$ whatever the scale. In particular, this term must be kept in the interfacial porous layer Ω_{fp} of thickness $d = O(d_p)$ and where ϕ varies continuously from ϕ_p to 1. But as soon as $L \geq 100\,d_p$, the approximation holds in Ω_p with $\mathrm{R}_{NS/F} \leq 1/100$ for $\phi_p \leq 0.95$ and the Brinkman viscous term is also negligible as discussed earlier. In that case, the flow in Ω_p is governed by Darcy-Forchheimer's equation (4).

Now, if the porous medium is anisotropic, Dupuit-Forchheimer's quadratic term takes a tensorial form as derived in [28]: $\boldsymbol{F}(\phi,|\boldsymbol{v}|)\cdot\boldsymbol{v}$, where the tensor $\boldsymbol{F}(\phi,|\boldsymbol{v}|)$ varies linearly with $|\boldsymbol{v}|$, so has the dimension of a velocity and is written in 2-D as :

$$\boldsymbol{F}(\phi,|\boldsymbol{v}|) := |\boldsymbol{v}|\,\boldsymbol{\kappa}(\phi) = |\boldsymbol{v}|\begin{pmatrix}\kappa_\tau(\phi) & \kappa_{\tau n}(\phi)\\ \kappa_{n\tau}(\phi) & \kappa_n(\phi)\end{pmatrix}. \qquad (13)$$

We also refer to [41] for the numerical solutions of the associated local closure problems showing that this tensor is positive but generally non-symmetric for ordered media in the so-called strong inertia regime of flow. Thus, the dimensionless tensor $\boldsymbol{\kappa}(\phi)$ is positive and possibly non-symmetric.

As a conclusion, the previous discussion justifies the momentum transport equation (3) in the transition porous region Ω_{fp}, which is derived by volume averaging for an heterogeneous porous medium in several works [27–29] and also in [30] for evolving heterogeneities.

3. The asymptotic interface model

The asymptotic model for the momentum transport is derived by integrating Eqs. (1), (3) and (5) over the thickness d of the interfacial layer Ω_{fp} using the constraint

$d/L \ll 1$ with $d = O(20\sqrt{K_p})$ [67] and related approximations up to $O(d/L)$. In the recent study [33], the thickness δ_B of Brinkman's viscous boundary layer is precisely investigated by filtered direct numerical simulations at the pore scale for different configurations of porous media. We also refer to [32] where the viscous boundary layer is theoretically calculated by WKB asymptotic expansions of which the convergence is proved. Since the transition layer Ω_{fp} due to the microstructure is included inside the Brinkman boundary layer, we have thus: $d \leq \delta_B$. Then, the averaged transfer is described at the fictive dividing interface Σ through suitable jump interface conditions at the first-order in $O(d/L)$.

For the sake of simplicity, we consider the simplest reasonable choice when the fictive interface Σ is centered inside Ω_{fp}, *i.e.* with the dimensionless coordinate $\xi := z_\Sigma/d = 0$. The modifications involved by $\xi \neq 0$ with $-1/2 \leq \xi \leq 1/2$ are detailed in [12] using non-centered approximations (see Remark 3) leading to a family of jump interface conditions depending on the location of Σ inside Ω_{fp}. In fact, the exact position of the interface inside Ω_{fp} is not of great importance for the present study since the model is derived hereafter up to the approximation order of $O(d/L)$. Therefore, compared to more sophiscated upscaling methods, the present simplified asymptotic theory considers the position of Σ as given *a priori*, as it is for the macroscopic problem to solve in Ω, and then the resulting approximate model is related to that given position up to $O(d/L)$.

It is also worth noting that at every step of the derivation of the model, a quantity is neglected only with respect to another term of the same physical meaning that is much larger. Hence, this allows us to assess that the global error remains of the order of $O(d/L)$ throughout the whole model[3]. We very often refer to [12] where the asymptotic modeling is extensively developed for the multi-dimensional but non-inertial viscous flow with arbitrary flow directions.

Let $\boldsymbol{n}$ be a unit normal vector on the interface Σ arbitrarily oriented from Ω_p to Ω_f and $\boldsymbol{\tau}$ be a unit tangential vector on Σ; see Figure 2. For any quantity ψ defined all over Ω, the restrictions on Ω_f or Ω_p are respectively denoted by $\psi^f := \psi_{|\Omega_f}$ and $\psi^p := \psi_{|\Omega_p}$. For a function ψ having a jump on Σ, let ψ^- and ψ^+ be the traces of ψ^p and ψ^f on each side of Σ, respectively. Following [68], the jump of ψ on Σ oriented by $\boldsymbol{n}$ and the arithmetic mean of traces of ψ are defined as reduced variables at the interface by

$$\begin{aligned} [\![\psi]\!]_\Sigma &:= \psi^+ - \psi^- = \left(\psi^f - \psi^p\right)_{|\Sigma}, \\ \overline{\psi}_\Sigma &:= \frac{1}{2}\left(\psi^+ + \psi^-\right) = \frac{1}{2}\left(\psi^f + \psi^p\right)_{|\Sigma}. \end{aligned} \tag{14}$$

Besides, for any quantity k, the arithmetic and harmonic means over the thickness of Ω_{fp} respectively are given by

$$\langle k \rangle(x) := \frac{1}{d}\int_{-d/2}^{d/2} k(x,z)\,\mathrm{d}z, \quad \langle k \rangle^h(x) := \left\langle \frac{1}{k} \right\rangle^{-1} \tag{15}$$

3.1. Jump interface conditions for the non-inertial flow

Before deriving jump conditions for the inertial flow, let us briefly recall the linear jump interface conditions for the stress and tangential velocity vectors at the interface Σ separating now the pure fluid domain Ω_f from the porous domain Ω_p, as derived in [12]:

$$\left\{ \begin{aligned} [\![\boldsymbol{v}\cdot\boldsymbol{n}]\!]_\Sigma &= 0 \\ \overline{\boldsymbol{\sigma}(\boldsymbol{v},p)\cdot\boldsymbol{n}}_\Sigma + \overline{p}_\Sigma\,\boldsymbol{n} &= \frac{2\mu}{d\,\phi_\Sigma}\,[\![\boldsymbol{v}]\!]_\Sigma \\ -[\![\boldsymbol{\sigma}(\boldsymbol{v},p)\cdot\boldsymbol{n}]\!]_\Sigma + \mu\,d\,\boldsymbol{K}_\Sigma^{-1}\cdot\overline{\boldsymbol{v}}_\Sigma &= d\,\langle\rho\,\boldsymbol{f}\rangle \end{aligned} \right. \tag{16}$$

where ϕ_Σ denotes an effective surface porosity on Σ and $\boldsymbol{K}_\Sigma$ is an effective surface permeability tensor on Σ.

The first equation in (16) indicates that there is no jump of the normal velocity across Σ. This is obtained by the average of the mass conservation equation $\boldsymbol{\nabla}\cdot\boldsymbol{v} = 0$ over the thickness of the interfacial layer Ω_{fp}, the additional tangential derivative term being of order of $O(Vd/L)$ and thus neglected in front of $[\![\boldsymbol{v}\cdot\boldsymbol{n}]\!]_\Sigma = O(V)$. We refer to [11] for higher-order asymptotic modelling of the flow in fractured porous media where the tangential derivatives are not neglected.

The second equation in (16) corresponds to the average of the viscous stress vector[4] from Eq. (5) and the scalar coefficient $2/d\,\phi_\Sigma$ can be related with the scaling $d = O(\sqrt{K_p})$ to the quantity $\alpha_\Sigma/\sqrt{K_p}$, where α_Σ denotes the non-dimensional slip coefficient, originally introduced semi-empirically in [2] for the 1-D channel flow with Darcy's law. Thus, this jump condition appears as a generalization for 2-D/3-D configurations with arbitrary flow directions of the popular Beavers and Joseph's tangential velocity jump which was early justified by volume averaging in [70, 71] and recently proved via homogenization by [10]. A simplified version was also justified with a statistical and volume averaging approach in [5] and proved via homogenization in [8]. According to the present theory, these two first conditions in Eq. (16) are not modified by including the inertial effects.

Remark 1 (Nonlinear Beavers-Joseph conditions). *Therefore, it does not seem physically meaningful to consider nonlinear versions of Beavers and Joseph's velocity jump condition as made by several authors, since the*

[3] With some obvious changes, the present theory can be applied to derive the macroscopic jump interface conditions for the flow between two porous media of different permeability, or with a non-Newtonian fluid.

[4] The derivation in [12] is carried out using the pseudo-stress vector: $\widetilde{\mu}\,\nabla\boldsymbol{v}\cdot\boldsymbol{n} - p\,\boldsymbol{n}$ on Σ instead of the full stress one $\boldsymbol{\sigma}(\boldsymbol{v},p)\cdot\boldsymbol{n}_{|\Sigma}$ with (5) that is more suitable for arbitrary flow directions [69]. However, the reader will be easily convinced that the contribution of $\nabla\boldsymbol{v}^T$ amounts to multiply the slip coefficient α_Σ by a factor 2 since all the tangential derivatives terms are neglected up to $O(d/L)$.

definition of the stress vector in Eq. (5) remains unchanged and linear whatever inertia or not. However, the case of non-Newtonian flows will result in a nonlinear Beavers-Joseph condition.

The last condition in (16) results from the averaging of the Darcy-Brinkman momentum equation, *i.e.* Eq. (3) with no inertial term, over the thickness d of the interfacial layer Ω_{fp}. This corresponds to the balance of forces across the interface Σ and this is the single equation which will be modified to take account of inertia terms included in Eq. (3). The tensorial quantity $d\,\boldsymbol{K}_\Sigma^{-1}$ can be rescaled and related to $\boldsymbol{\beta}_\Sigma/\sqrt{K_p}$, where $\boldsymbol{\beta}_\Sigma$ denotes the so-called Darcy friction tensor that is dimensionless. This condition can be viewed as a generalization for 2-D/3-D configurations with arbitrary flow directions of the shear stress jump condition originally derived by volume averaging in [6, 7, 72] for the 1-D flow with no tangential velocity jump or assuming no pressure jump [29].

Moreover, as argued in [12], the linear asymptotic model described by the set of equations (16) provides a suitable generalization for 2-D/3-D configurations with arbitrary flow directions of the interface conditions recently derived for the 1-D channel flow by volume averaging in [4] and including both shear stress and tangential velocity jumps.

Therefore, in agreement with the above discussion with the scaling $d = O(20\sqrt{K_p})$, we introduce the dimensionless scalar or tensorial slip and friction coefficients at the interface:

$$\begin{aligned} &\alpha_\Sigma := \frac{2\sqrt{K_p}}{d\,\phi_\Sigma} \quad \text{with} \quad \phi_\Sigma := \frac{1}{\langle \phi^{-1}\rangle} := \langle\phi\rangle^h \\ &\boldsymbol{\beta}_\Sigma := d\,\sqrt{K_p}\,\boldsymbol{K}_\Sigma^{-1} \quad \text{with} \quad \boldsymbol{K}_\Sigma := \langle \boldsymbol{K}(\phi)\rangle^h. \end{aligned} \tag{17}$$

Then, the asymptotic interface model (16) with a surface force $\boldsymbol{f}_\Sigma := d\,\langle \rho\,\boldsymbol{f}\rangle$ on Σ finally reads for the non-inertial regime and arbitrary flow directions up to $O(d/L)$:

$$\begin{cases} \qquad [\![\boldsymbol{v}\cdot\boldsymbol{n}]\!]_\Sigma = 0, \\ \overline{\boldsymbol{\sigma}(\boldsymbol{v},p)\cdot\boldsymbol{n}}_\Sigma + \overline{p}_\Sigma\,\boldsymbol{n} = \dfrac{\mu}{\sqrt{K_p}}\,\alpha_\Sigma\,[\![\boldsymbol{v}]\!]_\Sigma, \quad \text{on} \quad \Sigma. \\ -\,[\![\boldsymbol{\sigma}(\boldsymbol{v},p)\cdot\boldsymbol{n}]\!]_\Sigma + \dfrac{\mu}{\sqrt{K_p}}\,\boldsymbol{\beta}_\Sigma\cdot\overline{\boldsymbol{v}}_\Sigma = \boldsymbol{f}_\Sigma \end{cases} \tag{18}$$

Such a form similar to Eq. (18) was proposed earlier in [68, 73] to mathematically study the multi-dimensional fluid-porous flow and prove the solvability of the coupled Stokes/Brinkman or Stokes/Darcy problems.

Remark 2 (Over-determination with (18)). *Let us point out that the normal component of the second equation in (18) is not necessary to solve the problem since* $[\![\boldsymbol{v}\cdot\boldsymbol{n}]\!]_\Sigma = 0$ *is already given by the first equation. This can be used to determine the mean pressure* $\overline{p}_\Sigma$ *at the interface; see also [12] for the jump of pressure* $[\![p]\!]_\Sigma$ *at the interface. Thus, only the tangential component of this second equation is required with the first and third equations of (18) to prove that the whole fluid-porous coupled problem is well-posed. Indeed, the mathematical analysis of solvability is recently detailed in [74].*

Let us now derive separately the contribution of the additional inertial terms from Eq. (3) in Ω_{fp}, *i.e.* the Navier-Stokes nonlinear term and Dupuit-Forchheimer's quadratic inertial friction for the strong inertia regime of flow. The case of the weak inertia regime with a cubic inertial friction is also considered further.

3.2. Contribution of the Navier-Stokes nonlinear term

Let us set for convenience $\gamma(\phi) := 1/\phi$ and observe that $\phi_p \le \phi \le 1$ in Ω_{fp}. To respect the coherency of the modeling, this function should be cut off to zero in Ω_p, *i.e.* by taking $\gamma^p := \gamma(\phi_p) = 0$ in Ω_p, since the Navier-Stokes nonlinear term is neglected in Ω_p for $\phi_p \le 0.95$. Besides, we have using the trapezoidal quadrature formula:

$$\gamma_\Sigma := \langle\gamma(\phi)\rangle = \frac{1}{2}\,\left(\gamma^f + \gamma^p\right) + O(d^2) \approx \frac{1}{2}. \tag{19}$$

By integrating the Navier-Stokes nonlinear term in Eq. (3) over the thickness of Ω_{fp}, the density ρ being a constant, and applying the approximation Lemma 1 of the generalized average in Appendix A, we get:

$$\begin{aligned} &\int_{-d/2}^{d/2} \frac{1}{\phi}\,\boldsymbol{\nabla}\cdot\left(\frac{\rho}{\phi}\,\boldsymbol{v}\otimes\boldsymbol{v}\right)\,\mathrm{d}z \\ &= \rho\,\gamma_\Sigma \int_{-d/2}^{d/2} \boldsymbol{\nabla}\cdot\left(\gamma(\phi)\,\boldsymbol{v}\otimes\boldsymbol{v}\right)\,\mathrm{d}z + O\left(\rho\,\gamma_\Sigma^2\,V^2\,d^2/L^2\right). \end{aligned} \tag{20}$$

It clearly appears that the error term can be neglected up to $O(d/L)$. Then, it yields in the 2-D tensorial form up to the modeling error in $O(d/L)$:

$$\begin{aligned} &\rho\,\gamma_\Sigma \int_{-d/2}^{d/2} \boldsymbol{\nabla}\cdot(\gamma(\phi)\,\boldsymbol{v}\otimes\boldsymbol{v})\,\mathrm{d}z \\ &\qquad\qquad \approx \rho\,\gamma_\Sigma \begin{pmatrix} \partial_\tau(d\langle\gamma\,v_\tau^2\rangle) + [\![\gamma\,v_\tau\,v_n]\!]_\Sigma \\ \partial_\tau(d\langle\gamma\,v_\tau\,v_n\rangle) + [\![\gamma\,v_n^2]\!]_\Sigma \end{pmatrix}. \end{aligned} \tag{21}$$

However, the tangential derivative terms in both components are estimated as:

$$\begin{aligned} \left|\rho\,\gamma_\Sigma\,\partial_\tau(d\langle\gamma\,v_\tau^2\rangle)\right| &= O\left(\gamma_\Sigma^2\,\rho\,V^2\,\frac{d}{L}\right), \\ \left|\rho\,\gamma_\Sigma\,\partial_\tau(d\langle\gamma\,v_\tau\,v_n\rangle)\right| &= O\left(\gamma_\Sigma^2\,\rho\,V^2\,\frac{d}{L}\right), \end{aligned} \tag{22}$$

and they can be neglected up to $O(d/L)$ with respect to the jump terms which are of the order of $O(\gamma_\Sigma^2\,\rho\,V^2)$. Since $[\![v_n]\!]_\Sigma = [\![\boldsymbol{v}\cdot\boldsymbol{n}]\!]_\Sigma = 0$ [12] and thus $\boldsymbol{v}^f\cdot\boldsymbol{n} = \boldsymbol{v}^p\cdot\boldsymbol{n} = \boldsymbol{v}\cdot\boldsymbol{n}$, we get with Eq. (20) the approximation below up to $O(d/L)$:

$$\int_{-d/2}^{d/2} \frac{1}{\phi}\,\boldsymbol{\nabla}\cdot\left(\frac{\rho}{\phi}\,\boldsymbol{v}\otimes\boldsymbol{v}\right)\,\mathrm{d}z = \rho\,\gamma_\Sigma\,\boldsymbol{v}\cdot\boldsymbol{n}\,[\![\gamma\,\boldsymbol{v}]\!]_\Sigma. \tag{23}$$

Besides, by neglecting the Navier-Stokes nonlinear term in Ω_p, we have with $\gamma^p = 0$ and the definitions (14):

$$\gamma_\Sigma = \frac{1}{2}, \qquad [\![\gamma\, \boldsymbol{v}\cdot\boldsymbol{\tau}]\!]_\Sigma = \boldsymbol{v}^f \cdot \boldsymbol{\tau}_{|\Sigma}, \qquad [\![\gamma]\!]_\Sigma = \gamma^f - \gamma^p = 1.$$

Then Eq. (23) simplifies as:

$$\int_{-d/2}^{d/2} \frac{1}{\phi}\, \boldsymbol{\nabla}\cdot \left(\frac{\rho}{\phi}\, \boldsymbol{v}\otimes\boldsymbol{v}\right) \mathrm{d}z = \frac{1}{2}\, \rho\, \boldsymbol{v}\cdot\boldsymbol{n}\, \boldsymbol{v}^f. \tag{24}$$

We observe that this term is always null for the 1-D channel or shear flow, *i.e.* with $\boldsymbol{v}\cdot\boldsymbol{n} = 0$ at Σ, which is physically expected from the Poiseuille or Couette flow since the Navier-Stokes convection term vanishes. However, this term is generally non-zero for 2-D/3-D configurations with arbitrary flow directions.

3.3. Contribution of Dupuit-Forchheimer's term

Let us consider Dupuit-Forchheimer's quadratic term of Eq. (3) in Ω_{fp}, first written as:

$$\frac{\rho}{\sqrt{K_p}}\, \boldsymbol{F}(\phi,|\boldsymbol{v}|)\cdot\boldsymbol{v}, \quad \text{with} \quad \boldsymbol{F}(\phi,|\boldsymbol{v}|) := |\boldsymbol{v}|\, \boldsymbol{\kappa}(\phi).$$

By applying the approximation Lemma 1 of the generalized average in [12, Appendix B], the integral of this term over the thickness of Ω_{fp} yields with the scaling $d = O(\sqrt{K_p})$

$$\begin{aligned}\int_{-d/2}^{d/2} \frac{\rho}{\sqrt{K_p}}\, \boldsymbol{F}(\phi,|\boldsymbol{v}|)\cdot\boldsymbol{v}\, \mathrm{d}z \\ = \frac{\rho\, d}{\sqrt{K_p}}\, \langle \boldsymbol{F}(\phi,|\boldsymbol{v}|)\rangle \cdot \overline{\boldsymbol{v}}_\Sigma + O\left(\rho\, V^2\, \frac{d}{L}\right),\end{aligned} \tag{25}$$

and the error term can be neglected with respect to other terms in $O(\rho\, V^2)$.

Now, still using the approximation Lemma 1, we get:

$$\begin{aligned} d\langle \boldsymbol{F}(\phi,|\boldsymbol{v}|)\rangle &= \int_{-d/2}^{d/2} |\boldsymbol{v}|\, \boldsymbol{\kappa}(\phi)\, \mathrm{d}z \\ &= d\, \overline{|\boldsymbol{v}|}_\Sigma \langle \boldsymbol{\kappa}(\phi)\rangle + O\left(\|\langle \boldsymbol{\kappa}(\phi)\rangle\|_\infty\, V\, d^2/L\right). \end{aligned} \tag{26}$$

Let us define the positive tensor $\boldsymbol{\kappa}_\Sigma := \langle \boldsymbol{\kappa}(\phi)\rangle$ as the effective Dupuit-Forchheimer's friction tensor at Σ. Then, by replacing (26) in Eq. (25), it gives still using the scaling $d = O(20\sqrt{K_p})$:

$$\begin{aligned}\int_{-d/2}^{d/2} \frac{\rho}{\sqrt{K_p}}\, \boldsymbol{F}(\phi,|\boldsymbol{v}|)\cdot\boldsymbol{v}\, \mathrm{d}z \\ = \frac{\rho\, d}{\sqrt{K_p}}\, \overline{|\boldsymbol{v}|}_\Sigma\, \boldsymbol{\kappa}_\Sigma\cdot\overline{\boldsymbol{v}}_\Sigma + O\left(\|\boldsymbol{\kappa}_\Sigma\|_\infty\, \rho\, V^2\, \frac{d}{L}\right),\end{aligned} \tag{27}$$

and the error term can be still neglected. Hence, the approximation up to $O(d/L)$ of the integral across Ω_{fp} of Dupuit-Forchheimer's quadratic term in Eq. (3) reads

$$\int_{-d/2}^{d/2} \frac{\rho}{\sqrt{K_p}}\, \boldsymbol{F}(\phi,|\boldsymbol{v}|)\cdot\boldsymbol{v}\, \mathrm{d}z = \frac{\rho\, d}{\sqrt{K_p}}\, \overline{|\boldsymbol{v}|}_\Sigma\, \boldsymbol{\kappa}_\Sigma\cdot\overline{\boldsymbol{v}}_\Sigma. \tag{28}$$

3.4. Contribution of a power-law inertial term

More generally, let us now consider a power-law inertial term of the form:

$$\boldsymbol{F}_q(\phi,|\boldsymbol{v}|^q)\cdot\boldsymbol{v}, \quad \text{with} \quad \boldsymbol{F}_q(\phi,|\boldsymbol{v}|^q) := |\boldsymbol{v}|^q\, \boldsymbol{\kappa}(\phi),$$

with any real number $q > 0$. This term should be multiplied by a suitable quantity for dimensional reason to be included in Eqs. (3) and (4) instead of Dupuit-Forchheimer's term corresponding to $q = 1$. Then, using the same approximation procedure with Lemma 1, we get:

$$\int_{-d/2}^{d/2} \boldsymbol{F}_q(\phi,|\boldsymbol{v}|^q)\cdot\boldsymbol{v}\, \mathrm{d}z = \overline{|\boldsymbol{v}|^q}_\Sigma\, \boldsymbol{\kappa}_\Sigma\cdot\overline{\boldsymbol{v}}_\Sigma, \quad \text{on } \Sigma. \tag{29}$$

The cubic inertial term for the weak inertia regime corresponds to the case $q = 2$.

4. The nonlinear interface model for inertial flow

By incorporating the contributions of the inertial terms from Eqs (24) and (28) in the asymptotic interface model (18) for the non-inertial flow, we summarize below the nonlinear asymptotic model governing the 2-D/3-D inertial flow at the interface. By neglecting Brinkman's viscous term in Ω_p, within a suitable rescaling, it suffices to formally take the limit when the effective viscosity $\widetilde{\mu}^p \to 0$ inside Ω_p in the definition of the stress tensor (5) [32, 73], and thus the stress vector on the porous side of Σ reduces to the normal pressure force:

$$\boldsymbol{\sigma}(\boldsymbol{v},p)^p\cdot\boldsymbol{n}_{|\Sigma} = -p^p\, \boldsymbol{n}. \tag{30}$$

Indeed, the coupled limit problem when $\widetilde{\mu} \to 0$ is rigorously proved by a vanishing viscosity method in [73] or with a BKW asymptotic expansion to calculate the viscous boundary layer in [32] from the Stokes/Darcy-Brinkman problem to the Stokes/Darcy problem. We also refer to [33] for numerical investigations of the Brinkman boundary layer with pore-scale resolved simulations.

Since we have the scaling $d = O(20\sqrt{K_p})$, we introduce the dimensionless scalar or tensorial slip and friction coefficients at the interface:

$$\begin{aligned} &\alpha_\Sigma := \frac{2\sqrt{K_p}}{d\,\phi_\Sigma} \quad \text{with} \quad \phi_\Sigma := \frac{1}{\langle \phi^{-1}\rangle} := \langle\phi\rangle^h \\ &\boldsymbol{\beta}_\Sigma := d\,\sqrt{K_p}\, \boldsymbol{K}_\Sigma^{-1} \quad \text{with} \quad \boldsymbol{K}_\Sigma := \langle \boldsymbol{K}(\phi)\rangle^h \\ &\boldsymbol{\lambda}_\Sigma := \frac{d}{\sqrt{K_p}}\, \boldsymbol{\kappa}_\Sigma \quad \text{with} \quad \boldsymbol{\kappa}_\Sigma := \langle \boldsymbol{\kappa}(\phi)\rangle. \end{aligned} \tag{31}$$

Here, ϕ_Σ denotes an effective surface porosity on Σ, whereas $\boldsymbol{K}_\Sigma$ is an effective surface permeability tensor on Σ. Therefore, the nonlinear interface model with a surface

force $\boldsymbol{f}_\Sigma := d\,\langle \rho\,\boldsymbol{f}\rangle$ on Σ reads up to $O(d/L)$:

$$\left\{\begin{array}{l} [\![\boldsymbol{v}\cdot\boldsymbol{n}]\!]_\Sigma = 0, \\ \overline{\boldsymbol{\sigma}(\boldsymbol{v},p)\cdot\boldsymbol{n}}_\Sigma + \overline{p}_\Sigma\,\boldsymbol{n} = \dfrac{\mu}{\sqrt{K_p}}\,\alpha_\Sigma\,[\![\boldsymbol{v}]\!]_\Sigma, \\ \dfrac{1}{2}\,\rho\,\boldsymbol{v}\cdot\boldsymbol{n}\,\boldsymbol{v}^f - [\![\boldsymbol{\sigma}(\boldsymbol{v},p)\cdot\boldsymbol{n}]\!]_\Sigma \\ \quad + \dfrac{\mu}{\sqrt{K_p}}\,\boldsymbol{\beta}_\Sigma\cdot\overline{\boldsymbol{v}}_\Sigma + \rho\,\overline{|\boldsymbol{v}|}_\Sigma\,\boldsymbol{\lambda}_\Sigma\cdot\overline{\boldsymbol{v}}_\Sigma = \boldsymbol{f}_\Sigma \end{array}\right. \quad \text{on } \Sigma. \tag{32}$$

Remark 2 obviously holds also, as for (18), for the over-determination of the set of interface conditions (32).

Remark 3 (The case of Σ non-centered in Ω_{fp}). *For the sake of completeness, let us recall from [12] that when the dividing interface Σ is chosen non-centered inside Ω_{fp},* i.e. *for $\xi \neq 0$ (see Fig. 2), then all the mean quantities $\overline{\psi}_\Sigma$ in the interface conditions (18) or (32) must be replaced by their weighted counterpart $\overline{\psi}^w_\Sigma$ defined by:*

$$\overline{\psi}^w_\Sigma := \overline{\psi}_\Sigma + \xi\,[\![\psi]\!]_\Sigma, \qquad \textit{with} \quad -1/2 \le \xi \le 1/2. \tag{33}$$

Therefore, two special cases can be discussed: $\xi = 1/2$ giving $\overline{\psi}^w_\Sigma = \psi^f_{|\Sigma}$ where Σ is located at the top of the transition layer Ω_{fp} and $\xi = -1/2$ giving $\overline{\psi}^w_\Sigma = \psi^p_{|\Sigma}$ when Σ is at the bottom of Ω_{fp}; see [75].

Although the slip and friction coefficients should be estimated by experimental data or direct numerical simulations in ordered or random media, the present theory also provides correlations with respect to the porosity ϕ_p of the porous medium in Ω_p. These functions are calculated hereafter for isotropic tensors, $\boldsymbol{\beta}_\Sigma = \beta_\Sigma\,\boldsymbol{I}$ or $\boldsymbol{\lambda}_\Sigma = \lambda_\Sigma\,\boldsymbol{I}$, and depend on the scaling d/d_p chosen for the thickness of the transition layer Ω_{fp}, $d_p = O(\sqrt{K_p})$ being the mean diameter of solid particles or fibres. Indeed, we have chosen $d = O(10\,d_p)$ to derive the macroscopic momentum equation (3) in Ω_{fp}. Now, approximating the averaged quantities in Eqs. (31) by the trapezoidal rule which only includes the known values in Ω_f or Ω_p, we get:

$$\left\{\begin{array}{l} \alpha_\Sigma = \dfrac{2\sqrt{K_p}}{d}\,\langle\phi^{-1}\rangle \;\simeq\; \dfrac{\sqrt{K_p(\phi_p)}}{d}\left(1+\dfrac{1}{\phi_p}\right), \\ \beta_\Sigma \simeq \dfrac{d}{2\,\sqrt{K_p(\phi_p)}}, \\ \lambda_\Sigma = \dfrac{d}{\sqrt{K_p}}\,\langle\kappa(\phi)\rangle \;\simeq\; \dfrac{d\,\kappa(\phi_p)}{2\,\sqrt{K_p(\phi_p)}} \simeq \kappa(\phi_p)\,\beta_\Sigma. \end{array}\right. \tag{34}$$

It is easy to verify that these coefficients satisfy the required coherency at the asymptotics when $\phi_p \to 0$ or $\phi_p \to 1$ in Ω_p. The graphs of α_Σ and β_Σ for the scaling $d = 10\,d_p$ or $d = 10\,d_f$ are plotted in Fig. 7 and Fig. 8, respectively, using either Kozeny-Carman's correlation $K_p(\phi_p)$ for granular media [23, 24] or Happel-Langmuir's one for fibrous materials [25, 26]. The graph of λ_Σ is plotted in Fig. 9 using also the correlation of Ergun's coefficient $\kappa(\phi_p)$ from [38].

Remark 4 (On the inertial friction coefficient λ_Σ). *It is remarkable that λ_Σ at the interface is related to the stress jump coefficient β_Σ as $\lambda_\Sigma \simeq \kappa(\phi_p)\,\beta_\Sigma$ from (34). Therefore, the interface model for the inertial flow with $\xi = 0$ (*i.e. *Σ being centered in Ω_{fp}) only requires the surface coefficients $\alpha_\Sigma, \beta_\Sigma$ needed for the non-inertial flow and the Ergun's coefficient $\kappa(\phi_p)$ of the porous bulk Ω_p.*

Moreover, by choosing the interface Σ at the bottom of Ω_{fp}, i.e. *$\xi = -1/2$, it appears from the forthcoming study [75] that the interface conditions (32) degenerate to a generalized version of the stress jump condition of Ochoa-Tapia and Whitaker [6] with velocity continuity $\boldsymbol{v}^f = \boldsymbol{v}^p$ on Σ. Then, the single friction coefficient β_Σ is only required to calibrate the interface model for the inertial flow.*

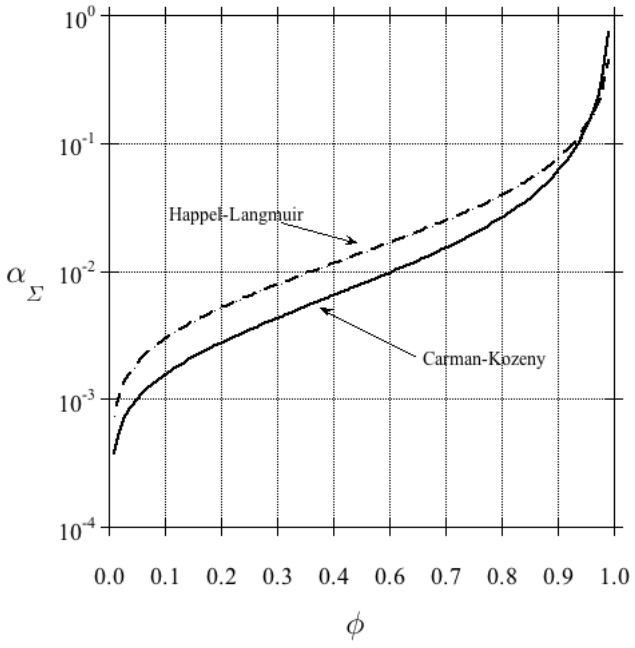

Figure 7: Slip coefficient α_Σ at the interface Σ in (34) for the scaling $d = 10\,d_p$ or $d = 10\,d_f$ and usual $K_p(\phi_p)$ correlations in Ω_p – Solid line: with Kozeny-Carman Eq. (6); Dashed line: with Happel-Langmuir Eq. (7).

5. The mechanical energy balance and dissipation

5.1. Energy balance for the fluid-porous inertial flow

Let us now derive the energy balance of the resulting macroscale coupled model (1,2,4) in the domain $\Omega := \Omega_f \cup \Sigma \cup \Omega_p$, *i.e.* the Navier-Stokes and Darcy-Forchheimer equations in Ω_f and Ω_p, respectively, supplemented by the interface model (32) on Σ. This will show that our model actually satisfies the energy theorem in mechanics at the macroscopic scale and that the conservation of kinetic energy holds.

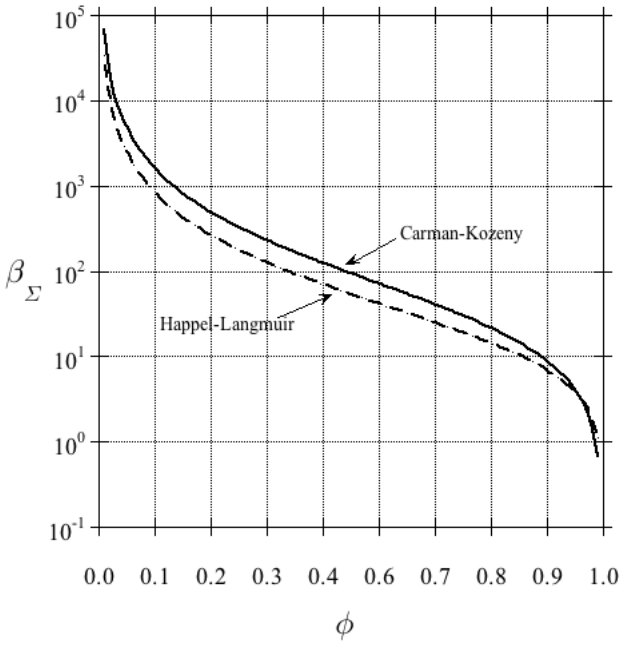

Figure 8: Friction coefficient β_Σ at the interface Σ in (34) for the scaling $d = 10\,d_p$ or $d = 10\,d_f$ and usual $K_p(\phi_p)$ correlations in Ω_p – Solid line: with Kozeny-Carman Eq. (6); Dashed line: with Happel-Langmuir Eq. (7).

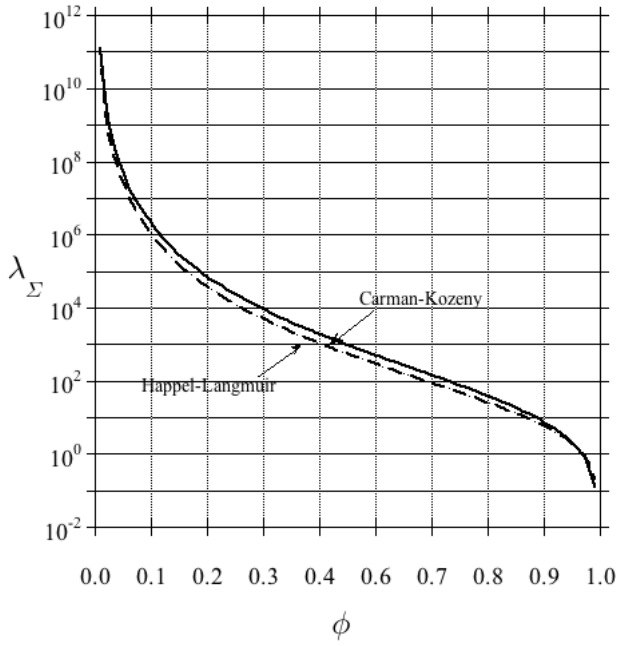

Figure 9: Coefficient of inertial friction $\lambda_\Sigma \simeq \kappa(\phi_p)\,\beta_\Sigma$ at the interface Σ in (34) for the scaling $d = 10\,d_p$ or $d = 10\,d_f$, $\kappa(\phi_p)$ correlation (10) from [37, 38] and usual $K_p(\phi_p)$ correlations in Ω_p – Solid line: with Kozeny-Carman Eq. (6); Dashed line: with Happel-Langmuir Eq. (7).

Without loss of generality, we assume null boundary conditions $\boldsymbol{v}^f_{|\Gamma} = 0$ and $\boldsymbol{v}^p \cdot \boldsymbol{n}_{|\Gamma} = 0$ at the external boundary Γ of Ω. Thus, all the boundary integrals on Γ will vanish with these homogeneous boundary conditions.

For the linear terms, we follow the mathematical analysis made in [74], see also [68, 73], for the well-posedness study of the fluid-porous Stokes/Darcy problem with the asymptotic interface conditions without inertia (16) and we include the contributions of all the nonlinear inertial terms. To deal with the nonlinear terms, it is more suitable to write the inertial term in the Navier-Stokes equation with constant density ρ in Ω_f as:

$$\rho\,(\boldsymbol{v}\cdot\nabla)\boldsymbol{v} = \rho\,(\nabla\times\boldsymbol{v})\times\boldsymbol{v} + \frac{1}{2}\,\nabla(\rho\,|\boldsymbol{v}|^2), \qquad (35)$$

which introduces Bernoulli's total pressure in the fluid Ω_f: $\pi^f := p^f + \rho\,|\boldsymbol{v}^f|^2/2$.

By taking L^2-scalar products of the motion equations with $\boldsymbol{v}$ in Ω_f and Ω_p, respectively, we use formally for sufficiently regular solutions standard integrations by parts and the boundary integrals on Γ vanish with homogeneous boundary conditions, as well as the integrals with divergence-free velocity terms. We have also the skew symmetry property:

$$\int_{\Omega_f} \left(\rho\,(\nabla\times\boldsymbol{v}^f)\times\boldsymbol{v}^f\right)\cdot\boldsymbol{v}^f\,\mathrm{d}x = 0. \qquad (36)$$

Using Eqs (35, 36) and $\boldsymbol{\nabla}\cdot\boldsymbol{v}^f = 0$, $\boldsymbol{v}^f_{|\Gamma} = 0$, we get with integration by parts:

$$\begin{aligned}\int_{\Omega_f} ((\rho\,\boldsymbol{v}^f\cdot\nabla)\boldsymbol{v}^f)\cdot\boldsymbol{v}^f\,\mathrm{d}x &= \int_{\Omega_f} \nabla\left(\frac{1}{2}\,\rho\,|\boldsymbol{v}^f|^2\right)\cdot\boldsymbol{v}^f\,\mathrm{d}x\\ &= -\int_{\Omega_f}\left(\frac{1}{2}\,\rho\,|\boldsymbol{v}^f|^2\right)\boldsymbol{\nabla}\cdot\boldsymbol{v}^f\,\mathrm{d}x\\ &\quad -\int_\Sigma \frac{1}{2}\,\rho\,|\boldsymbol{v}^f|^2\,\boldsymbol{v}^f\cdot\boldsymbol{n}\,\mathrm{d}s\\ &= -\frac{\rho}{2}\int_\Sigma |\boldsymbol{v}^f|^2\,\boldsymbol{v}\cdot\boldsymbol{n}\,\mathrm{d}s.\end{aligned} \qquad (37)$$

Hence, the contribution of the Navier-Stokes inertial term in Ω_f only involves the kinetic energy on Σ from Bernoulli's pressure.

Then, we follow the previous works [68, 73, 74] for the mathematical analysis of the fluid-porous flow without inertia. Using now the inertial interface conditions (32) instead of (18), we get after standard integrations by parts

the following energy balance:

$$\begin{aligned}\mu\int_{\Omega_f}|\nabla\boldsymbol{v}^f|^2\,\mathrm{d}x+\mu\int_{\Omega_p}(\boldsymbol{K}_p^{-1}\cdot\boldsymbol{v}^p)\cdot\boldsymbol{v}^p\,\mathrm{d}x\\ +\frac{\rho}{\sqrt{K_p}}\int_{\Omega_p}|\boldsymbol{v}^p|\,(\boldsymbol{\kappa}(\phi)\cdot\boldsymbol{v}^p)\cdot\boldsymbol{v}^p\,\mathrm{d}x\\ +\frac{\mu}{\sqrt{K_p}}\int_{\Sigma}\alpha_\Sigma\,[\![\boldsymbol{v}\cdot\boldsymbol{\tau}]\!]_\Sigma^2\,\mathrm{d}s\\ +\frac{\mu}{\sqrt{K_p}}\int_{\Sigma}(\boldsymbol{\beta}_\Sigma\cdot\overline{\boldsymbol{v}}_\Sigma)\cdot\overline{\boldsymbol{v}}_\Sigma\,\mathrm{d}s\\ +J_\Sigma=\int_{\Omega}\rho\,\boldsymbol{f}\cdot\boldsymbol{v}\,\mathrm{d}x+\int_{\Sigma}\boldsymbol{f}_\Sigma\cdot\overline{\boldsymbol{v}}_\Sigma\,\mathrm{d}s,\end{aligned}\tag{38}$$

where the energy quantity J_Σ gathers all the contributions of the nonlinear Navier-Stokes and Forchheimer inertial terms from the third interface condition in (32) on Σ and also includes the term (37). Therefore, we have:

$$\begin{aligned}J_\Sigma:=\rho\int_{\Sigma}\overline{|\boldsymbol{v}|}_\Sigma\,(\boldsymbol{\lambda}_\Sigma\cdot\overline{\boldsymbol{v}}_\Sigma)\cdot\overline{\boldsymbol{v}}_\Sigma\,\mathrm{d}s\\ +\frac{\rho}{2}\int_{\Sigma}\boldsymbol{v}\cdot\boldsymbol{n}\,\boldsymbol{v}^f\cdot\overline{\boldsymbol{v}}_\Sigma\,\mathrm{d}s-\frac{\rho}{2}\int_{\Sigma}|\boldsymbol{v}^f|^2\,\boldsymbol{v}\cdot\boldsymbol{n}\,\mathrm{d}s.\end{aligned}$$

By combining the last two terms using the definition of $\overline{\boldsymbol{v}}_\Sigma$ from (14), the quantity J_Σ finally reads:

$$\begin{aligned}J_\Sigma=\rho\int_{\Sigma}\overline{|\boldsymbol{v}|}_\Sigma\,(\boldsymbol{\lambda}_\Sigma\cdot\overline{\boldsymbol{v}}_\Sigma)\cdot\overline{\boldsymbol{v}}_\Sigma\,\mathrm{d}s\\ -\frac{\rho}{4}\int_{\Sigma}\left(|\boldsymbol{v}^f|^2-\boldsymbol{v}^f\cdot\boldsymbol{v}^p\right)\boldsymbol{v}\cdot\boldsymbol{n}\,\mathrm{d}s.\end{aligned}\tag{39}$$

Let us notice that the first term in the right-hand side of (39) is always positive whereas the second one is of arbitrary sign or vanishes if $\boldsymbol{v}^p=\boldsymbol{v}^f$ on Σ, *i.e.* when there is no jump of velocity at the interface.

5.2. Global dissipation of the coupled fluid-porous model

Now, we can prove the following result in Appendix C:

Theorem 1 (Sufficient condition for dissipation). *If the condition $\lambda_\Sigma\geq 1$ holds, then we have $J_\Sigma\geq 0$ and hence the global dissipation of the present model holds.*

This is at least satisfied within the porosity range of validity of the present Navier-Stokes/Darcy-Forchheimer macroscale model (1,2,4,32), i.e. $0<\phi_p\leq 0.95$, *as shown in Fig. 10 and Fig. 11 for a zoom.*

Indeed, introducing the ratio $R:=|\boldsymbol{v}^f|_\Sigma/|\boldsymbol{v}^p|_\Sigma\geq 1$, we recall that Saffman's approximation [5] assuming $|\boldsymbol{v}^p\cdot\boldsymbol{\tau}|\ll|\boldsymbol{v}^f\cdot\boldsymbol{\tau}|$ at the interface is generally not valid as soon as the porosity is large enough. Thus, only the condition $R\geq 1$ clearly holds but we do not have in general $R\gg 1$.

Then, it appears after calculations detailed in Appendix C that a simple sufficient condition to get $J_\Sigma\geq 0$ reads:

$$A:=\lambda_\Sigma\left(R^2+1\right)-2R\geq 0,\qquad\text{for any}\quad R\geq 1.\tag{40}$$

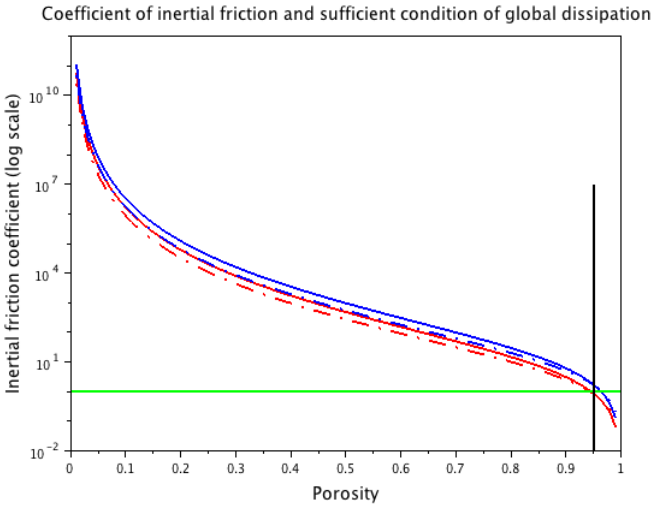

Figure 10: Coefficient of inertial friction $\lambda_\Sigma\simeq\kappa(\phi_p)\,\beta_\Sigma$ at the interface Σ in (34) for $\kappa(\phi_p)$ correlation (B.3) of [37, 38] and different correlations $K_p(\phi_p)$ in Ω_p or scalings of d: Kozeny-Carman Eq. (6) (solid line) for $d=5\,d_p$ (red) or $d=10\,d_p$ (blue) – Happel-Langmuir Eq. (7) (dashed line) for $d=5\,d_f$ (red) or $d=10\,d_f$ (blue) – Minimum coefficient for global dissipation: $\lambda_{min}=1$ (green) – Maximum porosity limit for ϕ_p: $\phi_{max}=0.95$ (black).

Then from (40), it follows the final sufficient condition for global dissipation:

$$\begin{aligned}&\lambda_\Sigma\geq 1\\ &\quad\Rightarrow\quad A\geq R^2+1-2R=(R-1)^2\geq 0\\ &\quad\Rightarrow\quad J_\Sigma\geq 0.\end{aligned}\tag{41}$$

As shown in Figures 10 and 11, the condition $\lambda_\Sigma\geq 1$ is clearly satisfied for the correlation of Ergun's coefficient $\kappa(\phi_p)$ given by [37, 38], but it also holds for other correlations like [40, 41], at least within the porosity range $\phi_p\leq 0.95$ of validity of the present Navier-Stokes/Darcy-Forchheimer model.

Thus we have always $J_\Sigma\geq 0$ with $\phi_p\leq 0.95$, which means that all the nonlinear terms at the interface have always a positive contribution to the dissipation of kinetic energy in the whole system Ω. Since, all the other terms in the left-hand side of Eq. (38) are also positive, we conclude that the present Navier-Stokes/Darcy-Forchheimer model is globally dissipative which assesses its stability and physical relevance[5]. Moreover, the condition $J_\Sigma\geq 0$ is also a strong argument to mathematically prove the global existence of weak solutions to this nonlinear flow model in 3-D, with no restriction on the size of the data.

[5] With the present theory and with no inertia at all in the porous region Ω_p, it does not seem possible to get the global dissipation with no restriction on the size of the data. Indeed, considering only the Navier-Stokes/Darcy problem, as made by some authors, would give $\lambda_\Sigma=0$. This does not enable us to control the kinetic energy at the interface Σ with the present interface conditions at $\xi=0$, nor discarding the first nonlinear term $\rho\,\boldsymbol{v}\cdot\boldsymbol{n}\,\boldsymbol{v}^f/2$ in (32) to get interface conditions that become then only linear.

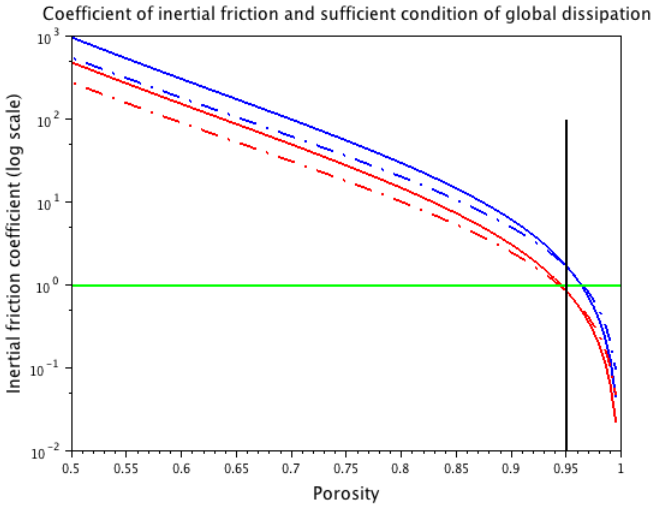

Figure 11: Zoom of Figure 10 with the same caption in the range of porosity $0.5 \leq \phi_p < 1$.

Remark 5 (Generalization for porosities $\phi_p > 0.95$). *The present interface model (32), its derivation and analysis of global dissipation can be extended with some modifications to larger porosities $\phi_p > 0.95$ of the permeable medium Ω_p, e.g. for fibrous porous media. In that case, considering now the Navier-Brinkman-Forchheimer equation (9) in Ω_p, the Navier-Stokes/Navier-Brinkman-Forchheimer model must be used for the free fluid and porous medium coupling together with a suitable modification of the interface conditions (32) on Σ. Then, the jump of velocity $[\![\boldsymbol{v}]\!]_\Sigma$ on the interface is small and can be neglected. Thus we have $\boldsymbol{v}^p \simeq \boldsymbol{v}^f$ on Σ and the second term in the right-hand side of (39) vanishes. Therefore, we get $J_\Sigma \geq 0$ and the global dissipation of the Navier-Stokes/Navier-Brinkman-Forchheimer model is also ensured. That is detailed in a forthcoming paper [76].*

6. Conclusion

Let us emphasize that the physically meaningful nonlinear interface model in the set of equations (32-34) is quite original since, to our knowledge, there exists in the literature no other multi-dimensional nonlinear macroscale model for the inertial flow with arbitrary flow directions over a permeable medium. Moreover, this clearly opens new perspectives to study turbulent flows at the fluid-porous interface.

References

[1] A. Bottaro, Flow over natural or engineered surfaces: an adjoint homogenization perspective, J. Fluid Mech. Perspectives 877 (P1) (2019) 1–91.

[2] G. S. Beavers, D. D. Joseph, Boundary conditions at a naturally permeable wall, J. Fluid Mech. 30 (1967) 197–207.

[3] B. Goyeau, D. Lhuillier, D. Gobin, M. G. Velarde, Momentum transport at a fluid-porous interface, Int. J. Heat Mass Transfer 46 (2003) 4071–4081.

[4] F. J. Valdés-Parada, C. G. Aguilar-Madera, J. A. Ochoa-Tapia, B. Goyeau, Velocity and stress jump conditions between a porous medium and a fluid, Adv. Water Res. 62 (2013) 327–339.

[5] P. G. Saffman, On the boundary condition at the surface of a porous medium, Stud. Appl. Math. 50 (2) (1971) 93–101.

[6] J. A. Ochoa-Tapia, S. Whitaker, Momentum transfer at the boundary between a porous medium and a homogeneous fluid I: theoretical development, Int. J. Heat Mass Transfer 38 (1995) 2635–2646.

[7] J. A. Ochoa-Tapia, S. Whitaker, Momentum transfer at the boundary between a porous medium and a homogeneous fluid II: comparison with experiment, Int. J. Heat Mass Transfer 38 (1995) 2647–2655.

[8] W. Jäger, A. Mikelić, On the interface boundary condition of Beavers & Joseph and Saffman, SIAM J. Appl. Math. 60 (4) (2000) 1111–1127.

[9] W. Jäger, A. Mikelić, Modelling effective interface laws for transport phenomena between an unconfined fluid and a porous medium using homogenization, Transp. Porous Media 78 (2009) 489–508.

[10] A. Brillard, J. E. Amrani, M. E. Jarroudi, Derivation of a contact law between a free fluid and thin porous layers via asymptotic analysis methods, Applicable Analysis 92 (4) (2013) 665–689.

[11] P. Angot, F. Boyer, F. Hubert, Asymptotic and numerical modelling of flows in fractured porous media, ESAIM: Math. Model. and Numer. Anal. 43 (2) (2009) 239–275.

[12] P. Angot, B. Goyeau, J. A. Ochoa-Tapia, Asymptotic modeling of transport phenomena at the interface between a fluid and a porous layer: Jump conditions, Phys. Rev. E 95 (6) (2017) 063302–(1–16).

[13] D. A. Nield, A. Bejan, in: Convection in Porous Media, 5th Edition, Springer (New York), 2017.

[14] M. Sahraoui, M. Kaviany, Slip and no-slip velocity boundary conditions at interface of porous plain media, Int. J. Heat Mass Transfer 35 (1992) 927–943.

[15] A. A. Hill, B. Straughan, Poiseuille flow in a fluid overlying a highly porous material, Adv. Water Res. 32 (11) (2009) 1609–1614.

[16] W. P. Breugem, B. J. Boersma, Direct numerical simulations of turbulent flow over a permeable wall using a direct and a continuum approach, Phys. Fluids 17 (2005) 025103.

[17] Q. Zhang, A. Prosperetti, Pressure-driven flow in a two-dimensional channel with porous walls, J. Fluid Mech. 631 (2009) 1–21.

[18] Q. Liu, A. Prosperetti, Pressure-driven flow in a channel with porous walls, J. Fluid Mech. 679 (2011) 77–100.

[19] M. E. Rosti, L. Cortelezzi, M. Quadrio, Direct numerical simulation of turbulent channel flow over porous walls, J. Fluid Mech. 784 (2015) 396–442.

[20] G. A. Zampogna, A. Bottaro, Fluid flow over and through a regular bundle of rigid fibres, J. Fluid Mech. 792 (2016) 5–35.

[21] H. Basser, M. Rudman, E. Daly, SPH modelling of multi-fluid lock-exchange over and within porous media, Adv. Water Res. 108 (2017) 15–28.

[22] U. Lācis, S. Bagheri, A framework for computing effective boundary conditions at the interface between free fluid and a porous medium, J. Fluid Mech. 812 (2017) 866–889.

[23] P. C. Carman, Fluid flow through granular beds, Trans. Inst. Chem. Eng. 15 (1937) 150–166.

[24] M. J. MacDonald, C. C. Chu, P. P. Guilloit, K. M. Ng, A generalized Blake-Kozeny equation for multi-sized spherical particles, AIChE J. 37 (1991) 1583–1588.

[25] J. Happel, Viscous flow relative to arrays of cylinders, AIChE J. 5 (1959) 174–177.

[26] G. W. Jackson, D. F. James, The permeability of fibrous porous media, Can. J. Chem. Eng. 64 (1986) 364–374.

[27] W. G. Gray, K. O'Neill, On the general equations for flow in porous media and their reduction to Darcy's law, Water Resources Res. 12 (2) (1976) 148–154.
[28] S. Whitaker, The Forchheimer equation: a theoretical development, Transp. Porous Media 25 (1996) 27–61.
[29] J. A. Ochoa-Tapia, S. Whitaker, Momentum jump condition at the boundary between a porous medium and a homogeneous fluid: inertial effects, J. Porous Media 1 (3) (1998) 201–217.
[30] P. Bousquet-Melou, B. Goyeau, M. Quintard, F. Fichot, D. Gobin, Average momentum equation for interdentritic flow in a solidifying columnar mushy zone, Int. J. Heat Mass Transfer 45 (17) (2002) 3651–3665.
[31] P. Angot, Analysis of singular perturbations on the Brinkman problem for fictitious domain models of viscous flows, Math. Meth. Appl. Sci. 22 (16) (1999) 1395–1412.
[32] P. Angot, G. Carbou, V. Péron, Asymptotic study for Stokes-Brinkman model with jump embedded transmission conditions, Asymptotic Analysis 96 (3-4) (2016) 223–249.
[33] R. Hernandez-Rodriguez, B. Goyeau, P. Angot, J. A. Ochoa-Tapia, Average velocity profile between a fluid layer and a porous medium: Brinkman boundary layer, Rev. Mexicana Ing. Química 19 (Sup. 1) (2020) 495–520.
[34] S. M. Hassanizadeh, W. G. Gray, High velocity flow in porous media, Transp. Porous Media 2 (6) (1987) 521–531.
[35] O. Coulaud, P. Morel, J.-P. Caltagirone, Numerical modelling of nonlinear effects in laminar flow through a porous medium, J. Fluid Mech. 190 (1988) 393–407.
[36] J. S. J. Andrade, U. M. S. Costa, M. P. Almeida, H. A. Makse, H. E. Stanley, Inertial effects on fluid flow through disordered porous media, Phys. Rev. Lett. 82 (26) (1999) 5249–5252.
[37] S. Ergun, Fluid flow through packed columns, Chem. Eng. Progr. 48 (2) (1952) 88–94.
[38] I. F. MacDonald, M. S. El-Sayed, K. Mow, F. A. L. Dullien, Flow through porous media: The Ergun equation revisited, Ind. Ing. Chem. Fundam. 18 (1979) 199–208.
[39] J. P. Du Plessis, Analytical quantification of coefficients in the Ergun equation for fluid friction in a packed bed, Transp. Porous Media 16 (1994) 189–207.
[40] T. D. Papathanasiou, B. Markicevic, E. D. Dendy, A computational evaluation of the Ergun and Forchheimer equations for fibrous porous media, Phys. Fluids 13 (2001) 2795–.
[41] D. Lasseux, A. A. A. Arani, A. Ahmadi, On the stationary macroscopic inertial effects for one phase flow in ordered and disordered porous media, Phys. Fluids 23 (7) (2011) 073103–(1–19).
[42] B. P. Muljadi, M. J. Blunt, A. Q. Raeini, B. Bijeljic, The impact of porous media heterogeneity on non-darcy flow behaviour from pore-scale simulation, Adv. Water Res. 95 (2016) 329–340.
[43] J. J. L. Higdon, G. D. Ford, Permeability of three-dimensional models of fibrous porous media, J. Fluid Mech. 308 (1996) 341–361.
[44] J. Dupuit, in: Etudes théoriques et pratiques sur le mouvement des eaux, Dunod (Paris), 1863.
[45] P. Forchheimer, Wasserbewegung durch boden, Zeit Ver. Deutsch. Ing. 45 (50) (1901) 1782–1788.
[46] S. Irmay, On the theoretical derivation of Darcy and Forchheimer formulas, J. Geophys. Res. 39 (1958) 702–707.
[47] G. Chauveteau, C. Thirriot, Régimes d'écoulement en milieu poreux et limite de la loi de Darcy, La Houille Blanche 2 (1967) 141–148.
[48] G. S. Beavers, G. M. Sparrow, D. E. Rodenz, Influence of bed size on the flow characteristics and porosity of randomly packed beds of spheres, J. Appl. Mech. 40 (1973) 655–660.
[49] R. C. Givler, S. A. Altobelli, A determination of the effective viscosity for the Brinkman–Forchheimer flow model, J. Fluid Mech. 158 (1994) 355–370.
[50] Z. Zeng, R. Grigg, A criterion for non-darcy flow in porous media, Transp. Porous Media 63 (1) (2006) 57–69.
[51] H. Ma, D. W. Ruth, The microscopic analysis of high Forchheimer number flow in porous media, Transp. Porous Media 13 (2) (1993) 139–160.
[52] S. Rojas, J. Koplik, Nonlinear flow in porous media, Phys. Rev. E 58 (4) (1998) 4776–4782.
[53] F. Thauvin, K. K. Mohanty, Network modeling of non-Darcy flow through porous media, Transp. Porous Media 31 (1) (1998) 19–37.
[54] T. Giorgi, Derivation of the Forchheimer law via matched asymptotic expansions, Transp. Porous Media 29 (2) (1997) 191–206.
[55] E. Marušić-Paloka, A. Mikelić, The derivation of a nonlinear filtration law including the inertia effects via homogenization, Nonlinear Anal. 42 (2000) 97–137.
[56] Z. Chen, S. L. Lyons, G. Qin, Derivation of the Forchheimer law via homogenization, Transp. Porous Media 44 (2) (2001) 325–335.
[57] D. W. Ruth, H. Ma, On the derivation of the Forchheimer equation by means of the averaging theorem, Transp. Porous Media 7 (3) (1992) 255–264.
[58] C. Soulaine, M. Quintard, On the use of a darcy-forchheimer like model for a macro-scale description of turbulence in porous media and its application to structured packings, Int. J. Heat Mass Transfer 74 (2014) 88–100.
[59] J.-C. Wodié, T. Lévy, Correction non-linéaire de la loi de Darcy, C. R. Acad. Sci. Paris 312 (1991) 157–161.
[60] J. B. Koch, J. C. Ladd, Moderate Reynolds number flows through periodic and random arrays of aligned cylinders, J. Fluid Mech. 340 (1997) 31–66.
[61] E. Skjetne, J.-L. Auriault, New insights on steady, non-linear flow in porous media, Eur. J. Mech. B/Fluids 18 (1) (1999) 131–145.
[62] M. Fourar, R. Lenormand, M. Karimi-Fard, R. Horne, Inertia effects in high-rate flow through heterogeneous porous media, Transp. Porous Media 60 (2005) 353–370.
[63] M. Panfilov, M. Fourar, Physical splitting of non linear effects in high-velocity stable flow through porous media, Adv. Water Res. 29 (2006) 30–.
[64] J. C. Ward, Turbulent flow in porous media, J. Hydraul. Div. ASCE 90 (1964) 1–12.
[65] D. D. Joseph, D. A. Nield, G. Papanicolaou, Nonlinear equation governing flow in a saturated porous medium, Water Resources Res. 18 (4) (1982) 1049–1052.
[66] D. A. Nield, Modelling fluid flow and heat transfer in a saturated porous medium, J. Appl. Math. Decision Sci. 4 (2) (2000) 165–173.
[67] F. J. Valdés-Parada, B. Goyeau, J. A. Ochoa-Tapia, Jump momentum boundary condition at a fluid-porous dividing surface: derivation of the closure problem, Chem. Engng Sci. 62 (2007) 4025–4039.
[68] P. Angot, A fictitious domain model for the Stokes/Brinkman problem with jump embedded boundary conditions, C. R. Math. Acad. Sci. Paris 348 (11-12) (2010) 697–702.
[69] I. P. Jones, Low Reynolds number flow past a porous spherical shell, Math. Proc. Cambridge Philos. Soc. 73 (1) (1973) 231–238.
[70] S. M. Ross, Theoretical model of the boundary condition at a fluid-porous interface, Amer. Inst. Chem. Engng J. 29 (5) (1983) 840–846.
[71] D. A. Nield, The Beavers-Joseph boundary condition and related matters: a historical and critical review, Transp. Porous Media 78 (2009) 537–540.
[72] M. Minale, Momentum transfer within a porous medium. II. Stress boundary condition, Phys. Fluids 26 (12) (2014) 123102.
[73] P. Angot, On the well-posed coupling between free fluid and porous viscous flows, Appl. Math. Lett. 24 (6) (2011) 803–810.
[74] P. Angot, Well-posed Stokes/Brinkman and Stokes/Darcy coupling revisited with new jump interface conditions, ESAIM: Math. Model. and Numer. Anal. 52 (5) (2018) 1875–1911. doi:10.1051/m2an/2017060.
[75] P. Angot, B. Goyeau, J. A. Ochoa-Tapia, A nonlinear stress jump interface condition with a single friction coefficient for the fluid-porous inertial flow, Transp. Porous Media (2020) (submitted).

[76] P. Angot, B. Goyeau, J. A. Ochoa-Tapia, A nonlinear interface model for the fluid-porous inertial flow in the whole range of porosity, in preparation.

Appendix A. Approximation result

The key practical result which is used several times in this study reads as follows. The proof is given in [12, Appendix B].

Lemma 1 (Approximations of generalized average).

Let the function $\psi : [-d/2, d/2] \to \mathrm{R}$ *be continuously differentiable and the function* $w : [-d/2, d/2] \to \mathrm{R}$ *be Lebesgue-integrable.*
Then we have:

$$\int_{-d/2}^{d/2} w(x)\,\psi(x)\,\mathrm{d}x = \langle w \rangle \int_{-d/2}^{d/2} \psi(x)\,\mathrm{d}x + O\left(\langle |w| \rangle \left\|\psi'\right\|_\infty d^2\right)$$
$$= d\,\langle w \rangle\,\overline{\psi}_\Sigma + O\left(\langle |w| \rangle \left\|\psi'\right\|_\infty d^2\right).$$

Appendix B. Different $\kappa - \phi$ correlations for Ergun's coefficient

Here, we summarize various widely used $\kappa - \phi$ correlations for Ergun's coefficient of Dupuit-Forchheimer's inertial resistance force. Most of the correlations are phenomenological and have been deduced from experiments. Recently, a few of them have been obtained using numerical simulations.

- Correlation by Ergun (1952) [37]: based on an implicit model of packed spheres

$$\kappa(\phi) \simeq 1.75\,\frac{(1-\phi)^{1/2}}{\phi^3}. \tag{B.1}$$

- Correlation by Irmay (1958) [46]: three-dimensional viscous flow in the tortuous channels of the medium composed by spherical grains

$$\kappa(\phi) \simeq \frac{0.045}{\phi^{3/2}}. \tag{B.2}$$

- Correlation by MacDonald *et al.* (1979) [38]: theoretical and experimental data with solid spheres

$$\kappa(\phi) \simeq 1.80\,\frac{(1-\phi)^{1/2}}{\phi^3}. \tag{B.3}$$

- Correlation by Papathanasiou *et al.* (2001) [40]: computational evaluations

$$\kappa(\phi) \simeq 0.08\,\frac{1-\phi}{\phi}. \tag{B.4}$$

- Correlation by Lasseux *et al.* (2011) [41]: numerical simulations

$$\kappa(\phi) \simeq 0.12\,\frac{(1-\phi)^{0.38}}{\phi^{2.04}}, \quad \text{for} \quad 0.3 \leq \phi \leq 0.75. \tag{B.5}$$

Appendix C. Proof of Theorem 1

The strategy is to get a non-negative lower bound of J_Σ given in (39). For sake of clarity, we consider the case of the isotropic tensor $\boldsymbol{\lambda}_\Sigma = \lambda_\Sigma \boldsymbol{I}$ with the scalar coefficient $\lambda_\Sigma > 0$. The general case of a symmetric positive definite tensor $\boldsymbol{\lambda}_\Sigma$ will easily follow by considering the classical minoration from Rayleigh's quotient:

$$(\boldsymbol{\lambda}_\Sigma \cdot \boldsymbol{v}) \cdot \boldsymbol{v} \geq \lambda_{min} \, |\boldsymbol{v}|^2, \quad \text{for all } \ \boldsymbol{v} \in \mathrm{R}^3,$$

where $\lambda_{min} > 0$ is the minimum eigenvalue of the matrix $\boldsymbol{\lambda}_\Sigma$. Then the result below holds using λ_{min} instead of λ_Σ.

Further from (39), we have the splitting below:

$$\begin{aligned} J_\Sigma &:= J_1 - J_2, \quad \text{with} \\ J_1 &:= \rho \int_\Sigma \overline{|\boldsymbol{v}|}_\Sigma \, (\boldsymbol{\lambda}_\Sigma \cdot \overline{\boldsymbol{v}}_\Sigma) \cdot \overline{\boldsymbol{v}}_\Sigma \, \mathrm{d}s \geq 0, \\ J_2 &:= \frac{\rho}{4} \int_\Sigma \left(|\boldsymbol{v}^f|^2 - \boldsymbol{v}^f \cdot \boldsymbol{v}^p \right) \boldsymbol{v} \cdot \boldsymbol{n} \, \mathrm{d}s. \end{aligned} \tag{C.1}$$

Now, the key idea is to introduce the ratio:

$$R := \frac{|\boldsymbol{v}^f|_\Sigma}{|\boldsymbol{v}^p|_\Sigma} \geq 1, \quad \text{on } \ \Sigma. \tag{C.2}$$

We recall that Saffman's approximation [5] assuming $|\boldsymbol{v}^p \cdot \boldsymbol{\tau}| \ll |\boldsymbol{v}^f \cdot \boldsymbol{\tau}|$ at the interface is generally not valid as soon as the porosity is large enough. Thus, only the condition $R \geq 1$ clearly holds since $|\boldsymbol{v}^p \cdot \boldsymbol{\tau}| \leq |\boldsymbol{v}^f \cdot \boldsymbol{\tau}|$ and also $\boldsymbol{v}^f \cdot \boldsymbol{n} = \boldsymbol{v}^p \cdot \boldsymbol{n} = \boldsymbol{v} \cdot \boldsymbol{n}$ on Σ. But we do not have in general $R \gg 1$.

Then, from one side using the definition of the arithmetic mean on Σ from (14), we have successively:

$$\begin{aligned} J_1 &= \rho \int_\Sigma \overline{|\boldsymbol{v}|}_\Sigma \, \lambda_\Sigma \, |\overline{\boldsymbol{v}}_\Sigma|^2 \, \mathrm{d}s \\ &= \frac{\rho}{8} \int_\Sigma \lambda_\Sigma \left(|\boldsymbol{v}^f| + |\boldsymbol{v}^p| \right) \left| \boldsymbol{v}^f + \boldsymbol{v}^p \right|^2 \, \mathrm{d}s \\ &= \frac{\rho}{8} \int_\Sigma \lambda_\Sigma \left(|\boldsymbol{v}^f| + |\boldsymbol{v}^p| \right) \left(|\boldsymbol{v}^f|^2 + |\boldsymbol{v}^p|^2 + 2 \, \boldsymbol{v}^f \cdot \boldsymbol{v}^p \right) \, \mathrm{d}s \\ &= \frac{\rho}{8} \int_\Sigma |\boldsymbol{v}^p|^3 \, \lambda_\Sigma \, (R+1) \left(R^2 + 1 + 2 \, \frac{\boldsymbol{v}^f \cdot \boldsymbol{v}^p}{|\boldsymbol{v}^p|^2} \right) \, \mathrm{d}s. \end{aligned}$$

Since $\boldsymbol{v}^f \cdot \boldsymbol{v}^p \geq 0$ on Σ, we get the minoration of J_1:

$$J_1 \geq \frac{\rho}{8} \int_\Sigma |\boldsymbol{v}^p|^3 \, \lambda_\Sigma \, (R+1) \left(R^2 + 1 \right) \, \mathrm{d}s. \tag{C.3}$$

From another side with the Cauchy-Schwarz inequality, we have the majoration of J_2:

$$\begin{aligned} |J_2| &\leq \frac{\rho}{4} \int_\Sigma \left(|\boldsymbol{v}^f|^2 + |\boldsymbol{v}^f| \, |\boldsymbol{v}^p| \right) |\boldsymbol{v} \cdot \boldsymbol{n}| \, \mathrm{d}s \\ &\leq \frac{\rho}{4} \int_\Sigma |\boldsymbol{v}^p|^3 \, \left(R^2 + R \right) \, \mathrm{d}s \\ &\leq \frac{\rho}{8} \int_\Sigma |\boldsymbol{v}^p|^3 \, 2R \, (R+1) \, \mathrm{d}s. \end{aligned} \tag{C.4}$$

Combining (C.3) and (C.4), we get the minoration of J_Σ below:

$$\begin{aligned} J_\Sigma &= J_1 - J_2 \\ &\geq \frac{\rho}{8} \int_\Sigma |\boldsymbol{v}^p|^3 \, (R+1) \left[\lambda_\Sigma \left(R^2 + 1 \right) - 2R \right] \, \mathrm{d}s. \end{aligned} \tag{C.5}$$

Then, it appears that a simple sufficient condition to get $J_\Sigma \geq 0$ reads:

$$\begin{aligned} A &:= \lambda_\Sigma \left(R^2 + 1 \right) - 2R \geq 0, \\ &\text{i.e.} \quad \lambda_\Sigma \geq \frac{2R}{R^2+1}, \quad \text{for any } \ R \geq 1. \end{aligned} \tag{C.6}$$

Since we have $0 < 2R/(R^2+1) \leq 1$ for all $R \geq 1$, the sufficient condition (C.6) is equivalent to the condition below:

$$\lambda_\Sigma \geq 1. \tag{C.7}$$

This ends the proof.

□